Proc. Estonian Acad. Sci. Eng., 2007, **13**, 4, 338–353

Seebeck's effect in micromachined thermopiles for infrared detection. A review

Alexander Graf[a], Michael Arndt[a] and Gerald Gerlach[b]

[a] Robert Bosch GmbH, Tübingerstrasse 123, 72703 Reutlingen, Germany; alexander.graf2@de.bosch.com

[b] Department of Electrical Engineering, Institute of Solid-State Electronics, TU Dresden, Helmholzstrasse 18, 01062 Dresden, Germany

Received 28 June 2007

Abstract. Beginning with the discovery of Seebeck, thermopiles have come increasingly under the spotlight of commercial infrared sensing. The constantly growing interest has motivated us to write an overview of micromachined thermopiles. The first part deals with the Seebeck effect and discusses the most important physical parameters. In the second part, the most important material systems, techniques and micromachined structures are discussed on the basis of different examples. We explain the motivation behind miniaturized thermopile detectors and give a functional explanation of physical interrelations. Finally, different applications are presented and discussed in terms of their future potential.

Key words: thermocouple, thermopile, semiconductor, temperature measurement.

1. INTRODUCTION

Towards the second decade of the 19th century Thomas Johann Seebeck began to examine the junction behaviour of electrically conductive materials. In 1821 he discovered that a small electric current will flow in a closed circuit of two dissimilar metallic conductors when their junctions are kept at different temperatures [1].

The discovery of Seebeck indirectly contributed to a revival of the debate on the nature of heat. Most physicists thought that radiant heat and light were different phenomena. But this incorrect belief was caused by the fact that it was not possible to measure small temperature differences with available instruments. Unfortunately, the small output voltage of Seebeck's thermocouples, some μV/K, primarily also prevented the measurement of very small temperature differences.

However, Nobili had the idea of connecting several bismuth-copper thermocouples in series, generating a higher and therefore measurable output voltage. The output voltage of such a thermopile structure linearly increases with the number of connected thermocouples. The higher sensitivity of this apparatus allowed more accurate temperature measurements. Towards the second half of the 19th century this led to the general acceptance that light and heat radiation differ only in their respective wavelengths [2].

Today thermopiles can be found in various applications for temperature or radiation measurements. There exist, for example, surface temperature sensors, gas sensors based on the Lambert–Beer law of absorption, and vacuum sensors. Up to now, the working principle of thermopiles has remained unchanged. But like all electronic devices, they have undergone the common trend of miniaturization. Therefore new fabrication methods have had to be developed. It was found that semiconductors are favourable materials not only because of the wealth of positive experiences in IC production. For the construction of thermopiles in the μm scale, they offer higher Seebeck coefficients and facilitate the use of micromachining processes. In recent years different semiconducting material systems have been explored. For technological and economic reasons, the common industrial system today is the CMOS thermopile, which consists of Al-Si thermocouples.

2. THE SEEBECK EFFECT IN SEMICONDUCTOR THERMOCOUPLES

Figure 1 presents a typical example of an open circuit thermocouple structure. According to Seebeck, the thermocouple consists of two different leads a and b. With the junction on a higher thermal potential than the open end, it generates an open circuit voltage. Seebeck's experiments showed that there must exist proportionality between the applied temperature difference ΔT and the output voltage V_{out}.

In fact, an electrical potential difference V_{a} is generated within any isolated conduction material that is subjected to a temperature gradient ΔT. The physical phenomenon is called the absolute Seebeck effect. The absolute Seebeck

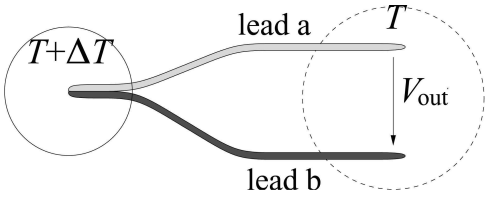

Fig. 1. Schematic drawing of an elementary thermocouple.

coefficient α_a is defined accordingly as the instantaneous rate of change of V_a [V] with respect to the temperature at a given temperature T_0 in K [3]:

$$\alpha_\mathrm{a} = \frac{\mathrm{d}V_\mathrm{a}}{\mathrm{d}T}\Big|_{T_0}. \tag{1}$$

Consequently, a thermovoltage being proportional to the applied temperature difference must arises at the open end of a thermocouple structure (Fig. 1):

$$\Delta V = \alpha_\mathrm{r}\Delta T = (\alpha_\mathrm{a,a} - \alpha_\mathrm{a,b})\Delta T, \tag{2}$$

where $\alpha_\mathrm{a,a}$ and $\alpha_\mathrm{a,b}$ are the absolute Seebeck coefficients of the materials a and b, respectively. The coefficient α_r is the effective or relative Seebeck coefficient of the thermocouple.

Generally, and without going deeper into thermodynamics, Pollock states in [3] that the Seebeck effect does not arise as a result of the junction of dissimilar materials, nor is it directly affected by the Thomson or Peltier effects; the latter two thermal effects are present only when current flows in a closed thermelectric circuit. Moreover, Ashcroft and Mermin describe the Seebeck effect as a consequence of the mean electron velocity [4]. The phenomenon implicates a gradient of the electrochemical potential $\Phi(T)$ [V] with respect to the temperature. Based on this, Sze expresses the output voltage of a thermocouple in [5] as

$$\Delta V = \left(\frac{\mathrm{d}}{\mathrm{d}T}\Phi_\mathrm{a}(T) - \frac{\mathrm{d}}{\mathrm{d}T}\Phi_\mathrm{b}(T)\right)\Delta T. \tag{3}$$

Herwaarden gives in [6] a more descriptive explanation of the absolute Seebeck effect in extrinsic non-degenerate silicon (Fig. 2). Following Eq. (3), he derives α_a as a superposition of electrical and thermal effects disturbing the semiconductor's energy band system. According to this, it can be concluded that the energy gap

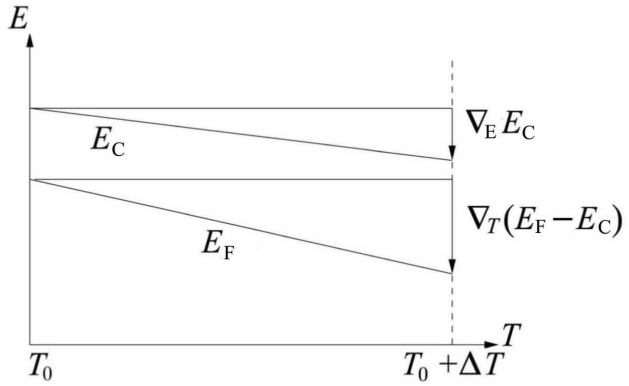

Fig. 2. Temperature dependence of the Fermi energy.

between the conduction band edge and the Fermi energy locally increases due to a temperature induced change in the Fermi–Dirac distribution ($\nabla_T(E_\mathrm{F} - E_\mathrm{C})$).

Additionally, a change of the conduction band energy E_c[eV] can be observed, which is the result of an electric field E, induced by a net diffusion current and by phonon-drag currents $\nabla_\mathrm{E} E_\mathrm{C}$. The phonon-drag current is a result of the net current of phonons, flowing towards the cold end of the silicon, pulling the charge carriers along with them.

These considerations lead to an equation, describing the absolute Seebeck coefficient in n-doped silicon:

$$\alpha_{\mathrm{a,n}} = -\frac{k}{q}\left[\ln\left(\frac{N_\mathrm{c}}{n}\right) + \frac{5}{2} + s_\mathrm{n} + \varphi_\mathrm{n}\right], \tag{4}$$

with N_c [1/cm^3] as the conduction band density of states, n [1/cm^3] the electron density, and k [J/K] the Boltzmann constant. The factor s_n is the exponent describing the relation between relaxation time and charge carrier energy [7] and φ_n is the contribution of acoustic phonons dragging charge carriers towards the cold side of the crystal. A corresponding term can be found for *p*-type semiconductors. In accordance, it can be found that the highest Seebeck coefficient is reached by materials which have only few charge carriers and which have at the same time a high charge carrier mobility [8,9]. Further considerations of the Seebeck effect in two-band semiconductors can be found in [10–12].

The Seebeck effect as it has been treated here is valid for bulk materials. Further effects such as grain size and grain boundary effects are found in thin-film structures. A good description of the effects in very thin films has been given by Salvadori et al. [13].

3. MICROMACHINED SEMICONDUCTOR THERMOPILES

Figure 3 shows a schematic drawing of a modern thermopile structure. Basically, it consists of N series-connected thermocouples, supported by a micromachined silicon membrane. The output voltage of the thermopile can be calculated as

$$V_\mathrm{out} = N\alpha_\mathrm{r}\Delta T. \tag{5}$$

In the past, two related demands led to an advancement in thermopile technology. On the one hand, there was a widespread interest in microelectronic devices. On the other hand, thermopile physics itself forced miniaturization in order to achieve higher detectivities D^*, expressed as

$$D^* = \frac{a\, t_\mathrm{tr}\, N\, \alpha_\mathrm{r}}{G\sqrt{1+\omega^2\tau_\mathrm{th}^2}}\sqrt{\frac{A_\mathrm{s}}{4\,k\,T\,R_\mathrm{i}}}. \tag{6}$$

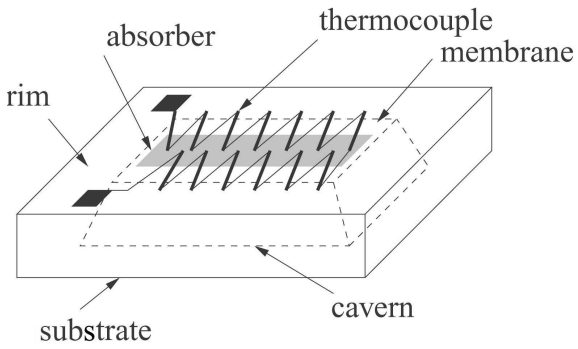

Fig. 3. Drawing of a bulk micromachined thermopile with anisotropically etched membrane.

Here a is the effective absorption, t_{tr} is the transparency of the radiation path, G is the thermal conductivity, τ_{th} is the thermal time constant, ω is the angular frequency of the modulated infrared source, A_{s} is the sensitive area of the detector and R_{i} is the internal resistance.

An effective increase of the detectivity D^* can be reached by a reduction of the thermal capacity for what the device has to be scaled down. This step becomes evident if we approximate Eq. (6) by weighing the thermal time constant against the thermal conductivity. The detectivity stays proportional to the square root of the active detector area divided by the thermal capacity. Keeping in mind that by scaling down a disk for a certain percentage, the surface area decreases with the square root, the miniaturization of the thermopile is an appropriate way to increase the overall detectivity.

Despite the long tradition of metal thermocouples, there are four main advantages that justify the use of semiconductors in thermopile fabrication.

1. Semiconductors offer a Seebeck coefficient that is about one or two orders of magnitude higher than that of metals.
2. The Seebeck coefficient strongly depends on the concentration of mobile charge carriers and the charge carrier mobility. Also taking into account that thermal noise is inversely proportional to the doping concentration, it becomes evident that the main characteristics of semiconducting thermopiles can be tuned by doping.
3. Semiconductor micromachining allows the thermal capacity to be reduced effectively by miniaturization.
4. Only semiconductor materials make it possible to produce thermopiles with high detectivity using a conventional IC process like the CMOS process.

Thus semiconductor thermopiles have the best potential to satisfy the demands on miniaturization and mass production. However, the capability of each thermopile strongly depends on the structure and the chosen material system. In order to illustrate the theory, the most important micromachined thermopile configurations for infrared detection will be presented.

3.1. Thermocouple configurations

Generally, two different thermopile configurations are reported in the literature. The respective thermocouples are deposited either in a one-layer [12,14−16] or a multilayer configuration [17,18]. The most common thermopile structure is the one-layer thermopile (Fig. 4). In this configuration, both thermocouple leads lie in a single plane one beside the other, deposited with conventional lithography processes. From a technological point of view, one-layer structures allow simple and fast processing because no additional layers are needed. The structure provides good thermal isolation due to its flatness.

In a multilayer configuration (Fig. 5), one thermocouple lead lies upon the other. They are separated by a thin insulating layer (e.g., photoresist). The insulating layer is removed by a photolithographic process only at the hot and cold ends of the first patterned thermoelectric film, forming small contact windows (Fig. 5) [18].

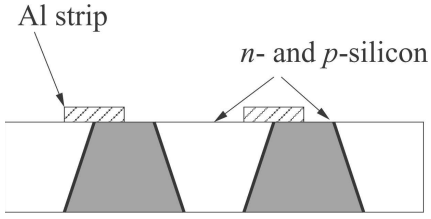

Fig. 4. One-layer thermopile with Al strip coupled thermocouples.

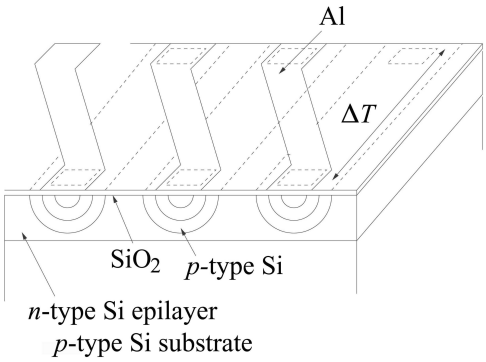

Fig. 5. Si-Al thin-film thermopile with diffusion implanted p-doped strips, interconnected by lift-off deposited Al leads.

3.2. Micromachined thermopile devices

3.2.1. Closed membranes

Closed micromachined membranes are structures commonly used in thermopile devices to isolate the heat from the cold contacts. The cold region, containing cold junctions of the thermopile, is formed by a wafer thick rim around the etched membrane. This rim serves not only as a heat sink, but also as suspension of the etched structure, as mechanical protection and for handling the sensor. A summary of the thermal properties of micromachined thermal sensors as well as some simulations are published by Simon et al. [19].

The hot region is in fact the absorber-covered membrane area within the radius of the hot junctions of the thermopile. The thermal resistance R_{th} [K/W] of a circular membrane is proportional to the logarithm of the ratio of the inner radius r_{i} to the outer radius r_{o} of the thermopile junctions. In practice, the thermal resistance is limited to 1/2 times the thermal sheet resistance R_{st} of the membrane [12,20,21]:

$$R_{\mathrm{th}} = \frac{1}{2\pi} \ln\left(\frac{r_{\mathrm{o}}}{r_{\mathrm{i}}}\right) R_{\mathrm{st}}. \tag{7}$$

In [16,22] the sensitivity of circular gas-filled thermopiles has been calculated. Figure 6 shows the cross-section of such a thermopile with cavity, thermocouples and absorber. In cylindrical coordinates, the steady-state temperature distribution from the receiving area to the heat sink is given by a differential equation of the Poisson type. The equation is based on Fourier's law of thermal conduction [23]:

$$\frac{\mathrm{d}^2(T - T_{\mathrm{e}})}{\mathrm{d}r^2} + \frac{1}{r}\frac{\mathrm{d}(T - T_{\mathrm{e}})}{\mathrm{d}r} - GR_{\mathrm{th}}(T - T_{\mathrm{e}}) = 0, \tag{8}$$

where T_{e} is the surrounding temperature.

Without knowing the exact solution of Eq. (8), it becomes evident that the thermopile characteristics can be influenced by the filling gas, as well as by the free path length within the device. Increasing G on the one hand leads to a reduced responsivity, but on the other hand makes the detector faster.

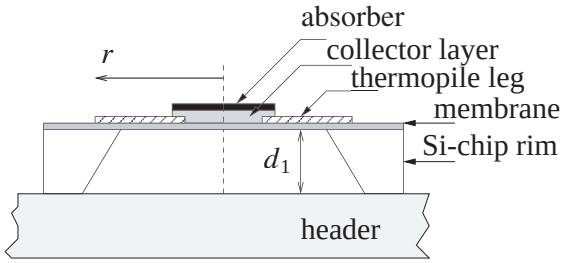

Fig. 6. Cross-section of a circular bulk-micromachined thermopile with its main functional components.

3.2.2. Microcantilever membranes

A further increase of the thermal resistance, compared with closed membrane thermopiles, can be reached by reducing the contact between membrane and silicon rim (Fig. 7). Unfortunately, this also reduces the mechanical stability of the device. However, thermopiles with cantilever beams are suitable for applications that require very high sensitivity. Typically, bulk-micromachined beam-type thermopiles are fabricated by an anisotropic etching process. For example, in [24,25] Sarro and van Herwaarden propose a bipolar process based on KOH etching. Figure 7 shows a schematic drawing of such a detector.

A careful analysis of the steady state temperature distribution is given by Elbel et al. [26]:

$$\frac{\mathrm{d}^2(T_{(x)} - T_\mathrm{e})}{\mathrm{d}x^2} - \frac{\varepsilon_\mathrm{c}\sigma A(T_{(x)}^4 - T_\mathrm{e}^4)}{\lambda V} - \frac{\xi A(T_{(x)} - T_\mathrm{e})}{\lambda V} = 0, \tag{9}$$

with T_e as the surrounding temperature, ε_c as the emissivity of the cantilever material, σ as the Stefan–Boltzmann constant, ξ as the heat transfer coefficient of the adjacent gas layers, λ as the mean thermal conductivity of the thin film stack, V as the detector volume and A as the beam surface area. The second and third terms in Eq. (9) denote the heat loss due to radiation and thermal conduction in gas and solid parts. By solving the differential equation, the interaction of the absorbing area and thermopile stripe length can be examined.

3.2.3. Surface-bulk micromachined thermopiles

Latest developments favor surface-bulk micromachined thermopiles, with which two main advantages over bulk-micromachined devices can be reached. First, the wafer is processed only from one side, reducing the complexity and duration of the fabrication process. Secondly, the thermopile can be hermetically sealed with one additional cap wafer. As a result, the thermopile is protected from environmental influences and operates under vacuum conditions, increasing the overall detectivity.

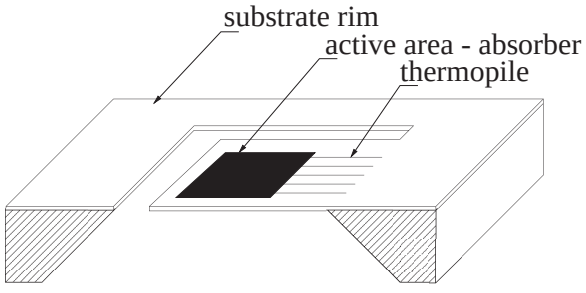

Fig. 7. Schematic drawing of an electrochemically etched beam-type thermopile.

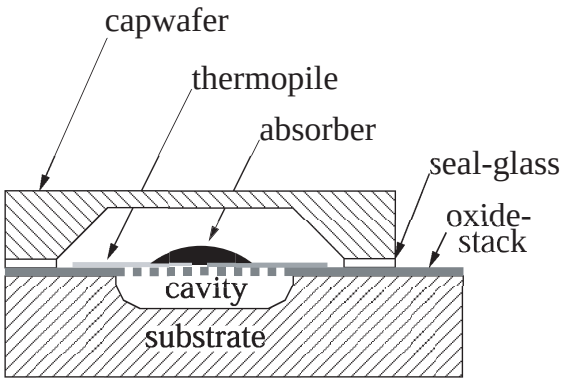

Fig. 8. Cross-section of the Bosch thermopile chip.

A typical example of a closed CMOS surface-bulk micromachined thermopile is shown in Fig. 8. It has been developed by Arndt et al. [27]. The device is based on a silicon substrate. First, multiple oxide and epilayers, forming membrane and thermocouples, are deposited on the substrate surface. In order to be able to access the substrate, the surface layers are perforated by anisotropic etching. The substrate under the surface layer is removed through these etched windows in an isotropic ClF_3 dry-etching process. Finally, the entire thermopile is hermetically sealed with a seal-glass bonded cap-wafer. With this technique, a very robust low-cost thermopile with high responsivity of about 80 V/W for automotive applications could be implemented.

4. APPLICATIONS

Today, micromachined thermopiles can be found in many different applications such as radiation temperature sensors and infrared gas detectors. Customer applications in particular have grown in recent years due to the beneficial characteristics of micromachined thermopiles.

For example, thermopiles do not have to be chopped or cooled, thus reducing the overall system complexity. In addition, the long-term stability and the fact that thermopiles are continuously miniaturized make them attractive for small stand-alone applications. Further advantages include insensitivity to vibrations and the lack of self-heating. Their potential to fulfill the demands of cheap and miniaturized electrical elements with high performance continues to open up markets for new sensor applications.

4.1. Remote temperature measurement

Remote temperature measurement is the main application of micromachined thermopiles [28]. They can be found for example in automobiles, household

appliances and medical instruments such as clinical ear thermometers. Their working principle remains the same and can be easily understood considering heat flow (Fig. 9).

In the case of thermal measurements, thermopiles can be compared with current meters. Instead of measuring an electrical current, they measure the heat flow, emitted by an object trying to reach thermal equilibrium with its surroundings. If the object temperature T_{obj} is higher than the thermopile temperature T_{tp}, the heat flow from the object warms up the thermopile membrane and generates a positive output voltage

$$U_{\mathrm{out}} = K(\varepsilon_{\mathrm{obj}}\, T_{\mathrm{obj}}^4 - \varepsilon_{\mathrm{tp}}\, T_{\mathrm{tp}}^4), \tag{10}$$

with K as a proportionality factor and $\varepsilon_{\mathrm{obj}}$ and $\varepsilon_{\mathrm{tp}}$ as emission coefficients of the surfaces of object and thermopile, respectively.

Recently, an increasing number of thermopile arrays has found application in infrared sensing. Two-dimensional arrays are widely used to measure the temperature distribution of a hot body. In contrast, one-dimensional(linear) arrays are used, for example, as position or motion detectors or remote potentiometers.

Figure 10 shows the example of a motion detector. Two linear thermopile arrays are arranged in a non-parallel mode.

Using output signals of the two sensor devices, the hot body can be detected. Additionally to commonly known motion detectors, such a system allows the

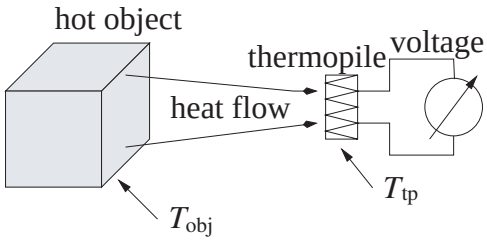

Fig. 9. Functional principle of a remote temperature sensor.

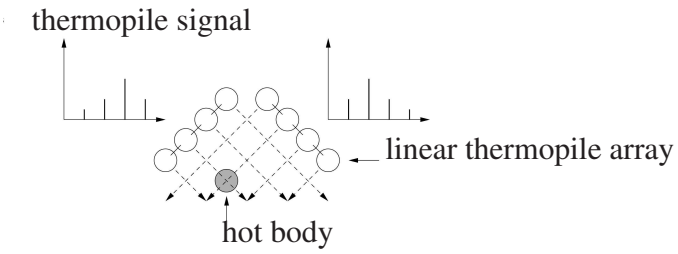

Fig. 10. Linear thermopile array as motion detecor.

position and the motion direction of the body to be calculated from the measurement data. Therefore correlations in the detector signals are analysed. With such a system more complex information is provided, for example, in security or driver assistance systems.

4.2. Gas sensors

Non-dispersive infrared (NDIR) sensors work in a similar way to remote temperature sensors. Generally, they both measure the amount of infrared radiation, incident on their active area. But the functional principle of a NDIR is based on the fact that gases with a constant dipole moment absorb electromagnetic radiation in specific wavelength ranges, particularly within the infrared spectrum. The total absorption is proportional to the number of photon–molecule interactions within the transmission path and can be expressed by the Lambert–Beers law of absorption

$$I = I_0 \, \mathrm{e}^{-\varepsilon c l}, \tag{11}$$

with I and I_0 as the radiation intensity $[\mathrm{W}/\mathrm{m}^2]$ after and prior to absorption, respectively, ε [1/ppm m] the specific absorptivity, c [ppm] the concentration of the species, and l [m] the length of the absorption path. By covering a radiation sensitive detector with a wavelength-selective filter, the radiation absorption of a specific gas can be measured.

The simplest kind of infrared gas sensor consists of a single detector element with a wavelength-selective filter and an infrared source, irradiating the detector element. Unfortunately, the sensor and especially its radiation source are subject to degradation. To avoid negative influence on the measurement results, most infrared gas sensors are equipped with a second measurement channel, monitoring aging effects (Fig. 11).

Arndt et al. [27,29] have used this approach together with the caped two-channel surface-bulk micromachined thermopile, described in section 3.2. The system setup comprises two different filter chips that are mounted on top of the thermopile chip.

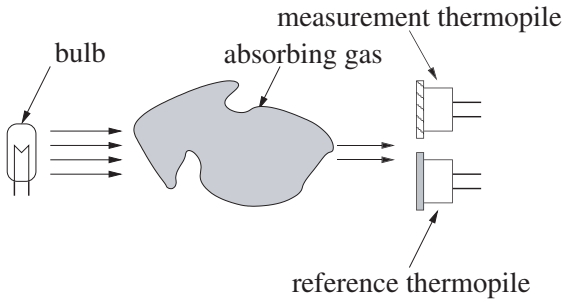

Fig. 11. Schematic drawing of a NDIR sensor with a two-channel detector.

One channel measures the radiation absorption due to CO_2, the other serves as a reference in the atmospheric window. Due to the very robust construction of the thermopile chip, degradation can almost be excluded. Typically, the sensor offers a resolution of about 200 ppm with an accuracy of $\pm 10\%$ and an absolute measurement range from 0 to 30.000 ppm.

Further developments investigate more flexible and cost saving systems [30]. Therefore, an ANDIR (Adaptive Non Dispersive Infrared) sensor with spectrally overlapping broad-band filters is being investigated [31]. As can be seen in Fig. 12, two different infrared filters include the three absorption bands of H_2O, HC and CO_2.

From a mathematical point of view, the system corresponds to a set of linear equations with the gas concentrations as the unknown variables. In constant driving mode, one equation for each detector can be generated. Thus the set of linear equations is underdetermined and cannot be solved. By taking measurements at a second infrared source temperature, a linearly independent data set is generated. This approach is based on the fact that the spectral intensity of a thermal radiation source changes with respect to Planck's law. Simulation and measurements show that the set of linear equations can thus be solved.

In practice, NDIR sensor systems are used as comfort sensors and due to their high reliability as safety sensors. Safety sensors measure the concentration of dangerous gases. A common application, for example, is the detection of increased concentrations of methane or carbon monoxide, which may be emitted by a gas cooker or an open fire.

Similarly, CO_2 sensors measure the concentration of carbon dioxide in air. An increased concentration of CO_2 can cause headaches and even a loss of consciousness. Hence, this kind of sensor is, for example, used to survey CO_2 climate control systems. A further application of the CO_2 sensor is regulation of the fresh air supply in closed rooms. In the case of air-conditioned rooms, the

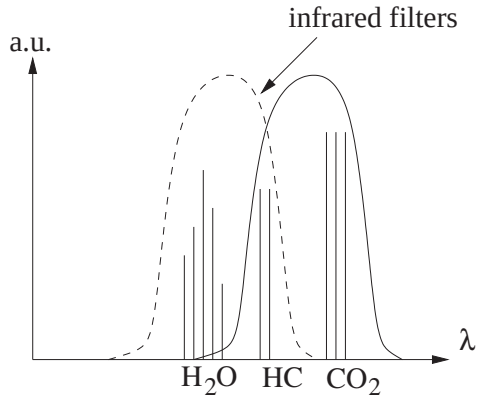

Fig. 12. Filter setup of a NDIR sensor with spectrally overlapping broad-band filters.

regulated supply of fresh air not only keeps the CO_2 concentration low but also allows the overall energy consumption of airconditioners to be reduced.

A comprehensive introduction to remote temperature sensors and NDIR sensors can be found in [28,32], where also some examples of thermopiles in medical applications and the usage of infrared sensors in food processing and farming are described. Additional non-infrared thermopile applications, such as thermal power or flow-sensors are described in [33−35].

5. OUTLOOK

During the last century, thermopiles changed from bulky metal devices to micromachined silicon infrared detectors. Some of the recent developments permit to envisage future trends.

Today, most thermopiles are housed in TO packages. Compared to velocity or gear rate sensors, where the state of the art package is a molded SMD frame, TO packages are still large, expensive and cause more complex production processes. The need for optics and thermal isolation prevented further developments up to now. However, recently presented surface-bulk micromachined thermopiles proved to be able to be packaged on the wafer level. These devices are small, mechanically stable, and thermally well isolated. In addition, optics, such as infrared transmission filters, can be deposited on the cap wafer. Further steps might also integrate refractive optics such as Fresnel lenses or gratings into the cap wafer. Both, wafer level packaging and integrated optics make a system that fulfills all requirements to be molded in an SMD package.

Other developments could deal with membrane structures. Evacuated thermopiles loose most of their thermal energy due to thermal conduction in the suspension membrane. The combination of a closed membrane and a cantilever structure would increase the thermal resistance between the silicon rim and the membrane by simultaneously keeping an adequate mechanical stability. In a first step, netlike membranes could be realized. Continuing investigations may finally lead to a further increase in thermal resistance by using micro-bridge structures.

Beyond the investigation of the physical detector properties, other activities may deal with the detector electronics. Generally, there can be found monolithic integrated detector electronics and hybrid systems with ASIC and detectors, separated into two different bonded chips. Both systems have their advantages. Due to the integrated amplifier stage, monolithic electronics offers a very high signal-to-noise ratio. Furthermore, integrated analogue to digital converters and serial communication ports offers a comfortable sensor device. On the other hand, hybrid systems are mostly designed as first-level amplifiers with an analogue signal output. On the costs of a slightly reduced signal-to-noise ratio and comfort, these systems offer a higher production yield and a higher flexibility. Up to know, it is an open question wether monolithic or hybrid systems will win, probably it might be a coexistence of both.

Apart from single detectors, thermopile arrays are also investigated. Today, there can already be found integrated linear and two-dimensional arrays with 16 to 32×32 elements. In future, arrays with even more elements can be expected. Nevertheless, it has to be questioned if thermopile arrays will achieve similar resolutions as micro-bolometer arrays.

It can be expected that thermopile arrays and SMD packaged thermopiles will lead to numerous new infrared sensing applications in the future. In the case of an array, applications such as two-dimensional temperature measurements, passive night vision systems, low-cost infrared cameras for security systems or multi-channel NDIR sensors for environment analysis, could be thought of. Additionally, it can be expected that SMD packaged single-element detectors will enter the consumer marked. One of the most attractive application is the usage of thermopiles as remote temperature sensors in mobile phones.

REFERENCES

1. Seebeck, T. J. Magnetische Polarisation der Metalle und Erze durch Temperatur-Differenz. *Abh. Deutsch. Akad. Wiss. Berlin*, 1822, 265–373.
2. Schettino, E. A new instrument for infrared radiation measurements: the thermopile of Macedonio Melloni. *Ann. Sci.*, 1989, **46**, 511–517.
3. Rowe, D. M. (ed.). *CRC Handbook of Thermoelectrics, Chapt. "General Principles and Theoretical Considerations"*. CRC Press, 1995.
4. Ashcroft, N. W. and Mermin, N. D. *Solid State Physics*. Saunders College, Philadelphia, 1976.
5. Sze, S. M. *Semiconductor Devices*. J. Wiley, New York, 2002.
6. Van Herwaarden, A. W. The Seebeck effect in silicon ICs. *Sensors Actuators*, 1984, **6**, 245–254.
7. Rowe, D. M. (ed.). *CRC Handbook of Thermoelectrics, Chapt. "Thermoelectric transport theory"*. CRC Press, 1995.
8. Dehe, A., Fricke, K. and Hartnagel, H. L. Infrared thermopile sensor based on AlGaAs-GaAs micromachining. *Sensors Actuators A*, 1995, **47**, 432–436.
9. Gaballe, T. H. and Hull, G. W. Seebeck effect in silicon. *Phys. Rev.*, 1955, **98**, 940–947.
10. Rittner, E. S. and Neumark, G. F. Theoretical bound on the thermoelectric figure of merit of two-band semiconductors. *J. Appl. Phys.*, 1963, **34**, 2071–2077.
11. Rowe, D. M. (ed.). *CRC Handbook of Thermoelectrics, Chapt. "Optimization of Carrier Concentration"*. CRC Press, 1995.
12. Van Herwaarden, A. W. and Sarro, P. M. Thermal sensors based on the Seebeck effect. *Sensors Actuators*, 1986, **10**, 321–346.
13. Salvadori, M. C., Vaz, A. R., Teixeira, F. S. and Cattani, M. Thermoelectric effect in very thin film Pt/Au thermocouples. *Appl. Phys. Lett.*, 2006, **88**.
14. Mzerd, A., Tchelibou, F., Sackda, A. and Boyer, A. Improvement of thermal sensors based on Bi_2Te_3, Sb_2Te_3 and $Bi_{0.1}Sb_{1.9}Te_3$. *Sensors Actuators A*, 1995, **47**, 387–390.
15. Lahiji, G. R. and Wise, K. D. A monolithic thermopile detector fabrication using integrated-circuit technology. In *International Electron Devices Meeting, Washington DC, Technical Digest*. 1980, 676–679.
16. Elbel, T. Miniaturized thermoelectric radiation sensor. *Sensors Materials A*, 1991, **3**, 97–109.

17. Elbel, T., Poser, S. and Fischer, H. Thermoelectric radiation microsensors. *Sensors Actuators A*, 1994, **42**, 493–496.
18. Völklein, F., Wiegand, A. and Baier, V. High-sensitivity radiation thermopiles made of Be-Sb-Te films. *Sensors Actuators A*, 1991, **29**, 87–91.
19. Simon, I. and Arndt, M. Thermal and gas sensing properties of a micromachined thermal conductivity sensor for the detection of hydrogen in automotive applications. *Sensors Actuators A*, 2002, **97–98**, 104–108.
20. Meijer, G. C. M. and Herwaarden, A. W. *Thermal Sensors, vol. 1*. Institute of Physics Publishing, Bristol, Philadelphia, 1994.
21. Van Herwaarden, A. W., van Duyn, D. C., van Oudheusden, B. W. and Sarro, P. M. Integrated thermopile sensor. *Sensors Actuators A*, 1989, **22**, 621–630.
22. Elbel, T. Miniaturized thermoelectric radiation sensor covering a wide range with respect to sensitivity or time constant. *Sensors Actuators A*, 1991, **27**, 653–656.
23. Simon, I. *Thermal Conductivity and Metal Oxide Gas Sensors*. PhD Thesis, Eberhard-Karls-Universität Tübingen, 2003.
24. Van Herwaarden, A. W., Sarro, P. M. and Meijer, G. C. Integrated vacuum sensor. *Sensors Actuators*, 1985, **8**, 187–196.
25. Sarro, P. M. and van Herwaarden, A. W. Silicon cantilever beams fabricated by electrochemically controlled etching for sensor applications. *J. Electrochem. Soc.*, 1986, **133**, 1724–1729.
26. Elbel, T., Lenggenhager, R. and Baltes, H. Model of thermoelectric radiation sensors made by CMOS and micromachining. *Sensors Actuators A*, 1992, **35**, 101–106.
27. Arndt, M. and Sauer, M. Spectroscopic carbon dioxide sensor for automotive applications. In *Proc. IEEE Sensors 2004*. Vienna, 2004, vol. 1, 252–255.
28. Schilz, J. *Thermoelectric Infrared Sensors (Thermopiles) for Remote Temperature Measurements; Pyrometry*. Whitepaper, PerkinElmer, July, 2000.
29. Sauer, M. and Arndt, M. Infrared carbon dioxide sensor and its applications in automotive air-conditioning systems. In *Advanced Microsystems for Automotive Applications* (Valldorf, J. and Gessner, W., eds.). 2005, vol. 8, 323–333.
30. Rubio, R., Santander, J., Sabate, N., Fonseca, L., Gracia, I., Moreno, M. and Marco, S. Thermopile sensor array for an electronic nose integrated non-selective NDIR detection system. In *Proc. Spanish Conference on Electron Devices*. Tarragona, 2005, 503–505.
31. Graf, A., Arndt, M. and Sauer, M. NDIR sensor with overlapping broad band filters and modulated IR source for gas analysis. In *Proc. 8th International Conference for Infrared Sensors and System (IRS)*. Nuremberg, 2006.
32. Schilz, J. *Applications of Thermoelectric Infrared Sensors (Thermopiles): Gas Detection by Infrared Absorption; NDIR*. Whitepaper, PerkinElmer, August, 2000.
33. Kodato, S., Wakabayashi, T., Zhuang, Q. and Uchida, S. New structure for DC-60 GHZ thermal power sensor. In *IEEE MTT-S International Microwave Symposium Digest*. New York, 1996, vol. 2, 871–874.
34. Van Oudheusden, B. W. Silicon thermal flow sensor with a two-dimensional direction sensitivity. *Measur. Sci. Technol.*, 1990, **1**, 565–575.
35. Oda, S., Anzai, M., Uematsu, S. and Watanabe, K. A silicon micromachined flow sensor using thermopiles for heat transfer measurements. *IEEE Trans. Instrum. Measur.*, 2003, **52**, 1155–1159.

Seebecki efekt infrapunakiirgust detekteerivates mikrovalmendatud termosammastes. Ülevaade

Alexander Graf, Michael Arndt ja Gerald Gerlach

Termosambad ehk -patareid said peagi pärast termoelektri avastamist Seebecki poolt kasvava tähelepanu objektiks kui tööstusliku potentsiaaliga infrapunakiirguse sensorid. Ülevaate esimeses osas on käsitletud Seebecki efekti rakendamisega seotud füüsikalisi probleeme, teises on analüüsitud materjale ja tehnoloogiaid, eriti just mikroskaalas valmistamisel. Samuti on vaadeldud termosammaste rakendusvõimalusi ja arutatud tulevikupotentsiaali.